The M_w 4.2 Delaware Earthquake of 30 November 2017

by Won-Young Kim, Mitchell Gold, Joseph Ramsay, Anne Meltzer, David Wunsch, Stefanie Baxter, Vedran Lekic, Phillip Goodling, Karen Pearson, Lara Wagner, Diana Roman, and Thomas L. Pratt

ABSTRACT

The 30 November 2017 Delaware earthquake with magnitude M_w 4.2 occurred beneath the northeastern tip of the Delmarva Peninsula near Dover, Delaware. The earthquake and its aftershocks provide an opportunity to evaluate seismicity in a passive margin setting using much improved coverage by high-quality permanent broadband seismometers at regional distance ranges in the central and eastern United States. This is the largest instrumentally recorded earthquake in Delaware, and it triggered a collaborative rapid-response effort by seismologists at five institutions along the mid-Atlantic. As a result of this effort, 18 portable seismographs were deployed in the epicentral region within 24 hrs of the mainshock. High-quality seismic recordings at more than 380 permanent regional broadband seismographic stations in the eastern United States show a remarkably small decrease in amplitude with distance between 800 and 2000 km. The mainshock focal mechanism shows predominantly strike slip with a significant thrust component. The orientation of the subhorizontal P axis is consistent with that of earthquakes in the nearby Reading-Lancaster seismic zone in Pennsylvania, but the trend is rotated counterclockwise about 45° from that of the M_w 5.8 Mineral, Virginia, earthquake. We detected small aftershocks below the normal event detection threshold using a waveform cross-correlation detection method. This demonstrated the effectiveness of this approach for earthquake studies and hazard evaluation in the eastern United States. Based on their waveform similarities, repeating earthquakes with magnitudes greater than 1.5 are detected in 2010, 2015, and 2017. Although there is a large time interval between events, 5 and 2.2 yrs, respectively, the events occur within a spatially tight cluster located near the 2017 Dover, Delaware, earthquake mainshock.

Electronic Supplement: Peak amplitude and instrumental intensity maps of the 30 November 2017 Delaware earthquake.

INTRODUCTION

On 30 November 2017, a moderate earthquake of magnitude M_w 4.2 (this study) occurred about 10 km northeast of Dover, Delaware, beneath the west coast of Delaware Bay (Fig. 1). The earthquake was felt throughout Delaware and in neighboring New Jersey, Maryland, and Pennsylvania, and the ground motion near the epicenter attained a maximum intensity of V (modified Mercalli intensity [MMI] scale), moderate shaking (Community Internet Intensity Map [CIIM], see Data and Resources). Light ground shaking was reported in Wilmington, Baltimore, and Philadelphia and as far away as New York City and Washington, D.C. ("Did You Feel It?," see Data and Resources). This event is the largest magnitude earthquake in Delaware at least in the past 150 yrs of record. The location and magnitude of the event were determined by the Lamont Cooperative Seismographic Network (LCSN) operated by more than 40 partner educational organizations in the northeastern United States and led by the Lamont–Doherty Earth Observatory (LDEO).

The seismic waves generated by the 2017 Delaware earthquake were well recorded by broadband seismographic stations in the central and eastern United States (CEUS). Although the Atlantic Ocean occupies the vast majority of area to the east of the hypocenter, more than 380 broadband seismographic stations from distances of 70 to 2800 km provided regional *Lg*-wave peak amplitude measurements with signal-to-noise ratio greater than 2. That the event was so well recorded is largely due to funding from the 2009 American Recovery and Reinvestment Act that allowed upgrading nearly all existing seismic stations in the eastern United States in 2010 and the continued deployment of new broadband stations by regional networks. The retention of 159 temporary (18-month deployment) USArray Transportable Array (TA) stations of the EarthScope project supported with National Science Foundation and U.S. Geological Survey (USGS) funds beginning in 2013 helped fill the gap in seismic station coverage in the eastern United States.

doi: 10.1785/0220180124

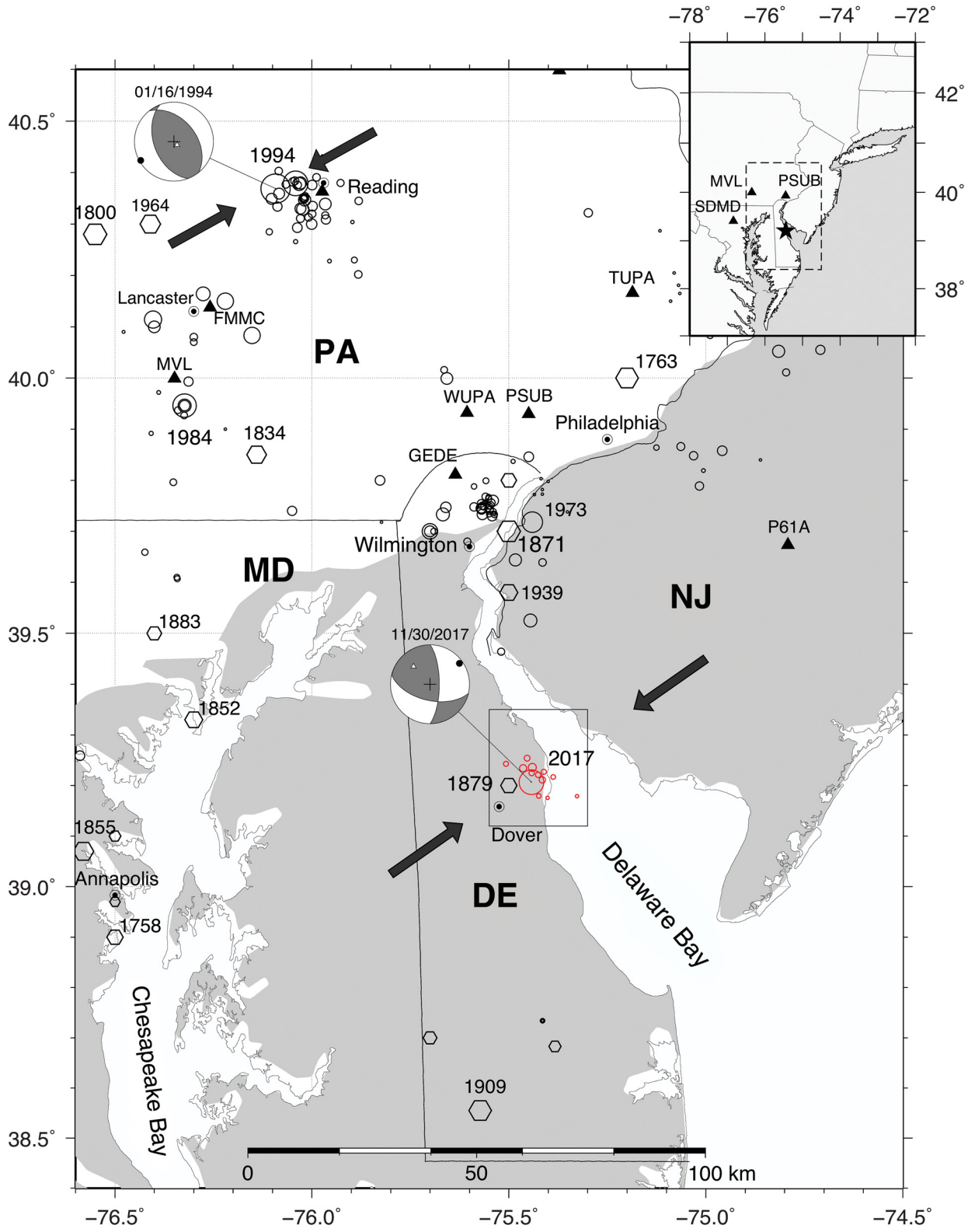

▲ **Figure 1.** Historical earthquakes that occurred in and around Delaware since 1785 from earthquake catalogs are plotted with hexagons; earthquakes since 1972 from Lamont Cooperative Seismographic Network catalog are plotted with circles. Permanent seismographic stations used to locate small earthquakes around Delaware are plotted with solid triangles. 1871 is the epicenter of the largest known earthquake (M 4.1) in Delaware, and 1879 is an M 3.3 earthquake that occurred close to the 2017 Delaware event. 1984 M 4.1 Lancaster, Pennsylvania, and 1994 M 4.6 Reading, Pennsylvania, earthquake sequences are indicated. Focal mechanism of the mainshock and trend of the subhorizontal P axis is indicated by thick arrows. Shaded area is Atlantic Coastal Plain strata covering bedrock.

The 2017 Delaware earthquake presents an opportunity for detailed study of a mainshock–aftershock sequence in a passive margin setting. The earthquake was followed by a rapid deployment of portable seismic stations by research and educational institutions in the region using limited resources but a collaborative effort. Within 24 hrs of the mainshock, 18 stations were deployed in the epicentral area on both shores of Delaware Bay. These local network stations operated for six weeks during the coldest winter in recent years. This article focuses on a description of the mainshock of the 2017 Delaware earthquake and analyses of seismic data recorded on the permanent seismographic stations in the mid-Atlantic States. More thorough analyses of the aftershock data are underway. The data from the temporary deployment are archived at the Incorporated Research Institutions for Seismology Data Management Center (see Data and Resources).

GEOLOGIC SETTING

The crust in the Delaware Bay region of the mid-Atlantic United States consists predominantly of Paleozoic and older crystalline and metamorphic rocks of the eastern U.S. Piedmont overlain unconformably by relatively unconsolidated sediments of the Atlantic Coastal Plain (Horton *et al.*, 1991; Volkert *et al.*, 1996). The epicenter is also near an inferred Mesozoic rift basin known primarily from scattered drill holes in the area. The Coastal Plain sequence onlaps the Cretaceous erosional surface at the top of the basement rocks to produce a landward-thinning wedge of sedimentary strata. In the epicentral area of the 2017 earthquake, the Coastal Plain strata have thicknesses in the 600- to 1200-m range (Volkert *et al.*, 1996). The surficial geology of the epicenter is underlain by extensive Holocene marsh deposits that are structureless to finely laminated organic-rich clay and silt-size sediments containing discontinuous peat beds. The marsh deposits can be up to ~12 m thick (Ramsey, 2007).

In the Washington, D.C. area, the Coastal Plain strata have been shown to substantially amplify ground shaking from the 2011 Mineral, Virginia, earthquake, resulting in higher intensities of ground shaking (Hough, 2012) and likely contributing to damage in Washington, D.C., from the 2011 earthquake (e.g., Wells *et al.*, 2015; Pratt *et al.*, 2017). This amplification suggests that earthquakes in the Dover area larger than the 2017 event could cause greater damage than might be expected for a given earthquake magnitude. Understanding active faults and the potential for future earthquakes are important goals for earthquake hazard assessments in the region. The 2014 USGS seismic hazard model shows relatively low hazard in the Dover area (Petersen *et al.*, 2014).

HISTORICAL SEISMICITY IN DELAWARE AND THE SURROUNDING REGION

Earthquake catalogs indicate that the 2017 Delaware shock is the largest magnitude event in Delaware since historical records began. According to the earthquake catalog compiled by the Delaware Geological Survey (DGS; see Data and Resources), an earthquake on 9 October 1871 beneath the Delaware River near Wilmington was the largest known earthquake in the state (maximum intensity VII; Stover and Coffman, 1993; Baxter, 2000; see Fig. 1 and Table 1). The 1871 earthquake caused damage in Wilmington as chimneys toppled and windows shattered, and it caused some damage in New Castle, Delaware, and in Oxford, Pennsylvania. Whereas DGS assigned a magnitude 4.1 for the 1871 earthquake based on damage reports, the Electric Power Research Institute (EPRI) (2012) put expected moment magnitude of 3.4, but the smaller amount of damage in the 2017 earthquake raises the possibility that the 1871 earthquake may have been larger (see Table 1). A magnitude $m_{b(Lg)}$ 3.8 earthquake occurred on 28 February 1973 across the river from Wilmington beneath the New Jersey side of Delaware Bay and the Delaware River (Fig. 1). That earthquake was felt widely in Delaware, New Jersey, and Pennsylvania. A magnitude 3.3 earthquake also occurred on 26 March 1879 at a location close to the 2017 event (Fig. 1 and Table 1).

Earthquakes with moment magnitude ranging from 3.1 to 3.8 that occurred near Annapolis, Maryland, along the western shore of the Chesapeake Bay are reported in the historical catalog (Table 1; EPRI, 2012), but the area has shown negligible seismicity since the nineteenth century (Fig. 1 and Table 1).

Several significant earthquakes have occurred within a 150-km radius of the 2017 Delaware event since the mid-1970s, when seismic stations began to be deployed to monitor earthquakes around proposed nuclear power plant sites in the eastern United States and earthquake catalogs started to become more complete. For example, a magnitude $m_{b(Lg)}$ 4.1 earthquake occurred on 23 April 1984, near Marticville (10 km south of MVL) in southern Lancaster County, Pennsylvania, that caused minor damage in Conestoga and other villages in the vicinity. This earthquake was felt over a large area and as far away as Connecticut and Virginia (Armbruster and Seeber, 1987; Fig. 1). On 16 January 1994, a magnitude M_w 3.9 foreshock preceded a magnitude M_w 4.6 mainshock near Wyomissing, 10 km west of Reading, Pennsylvania (Table 1; Du *et al.*, 2003). The mainshock produced intensity VI–VII effects near the epicenter and caused damage estimated at approximately $2 million U.S. (Seeber *et al.*, 1998). At the time, this was the most damage from an earthquake in the eastern United States since the 1944 Cornwall-Massena earthquake ($M_w \sim 5.8$) in New York. However, the 1994 event caused significantly less damage than the estimated economic losses ($200–$300 million U.S.) from the 2011 M_w 5.8 Mineral, Virginia, earthquake. The hypocenters of aftershocks of the 1994 earthquake were confined to the upper 2.5 km of the Earth's crust, a very shallow depth for earthquakes (Seeber *et al.*, 1998). On 26 August 2003, a magnitude M_L 3.5 earthquake originated at a shallow depth below the Delaware River near the towns of Milford, New Jersey, and Upper Black Eddy, Pennsylvania.

Although the 2017 Delaware earthquake is farther down Delaware Bay than most of these past earthquakes, people

Table 1
Significant Earthquakes in and around Delaware

Date (yyyy/mm/dd)	Time (hh:mm:ss)	Latitude (°N)	Longitude (°W)	Magnitude	Maximum Intensity*	Location†
1758/04/25	02:30:00	38.90	76.50	3.3‡		Annapolis, Maryland
1763/10/13	13:13:00	40.00	75.20	4.0‡		Philadelphia, Pennsylvania
1800/11/20	09:45:00	40.28	76.55	4.1‡		Hershey, Pennsylvania
1834/02/05	22:30:00	39.85	76.14	3.7‡		Millersville, Pennsylvania
1852/02/16	06:00:00	39.33	76.30	3.5‡		Middle River, Maryland
1855/06/28	00:18:00	39.07	76.58	3.8‡		Severna Park, Maryland
1871/10/09	14:40:00	39.7	75.5	4.1§	VII	Wilmington, Delaware
1879/03/26	12:30:00	39.2	75.5	3.3§	IV-V	Dover, Delaware
1883/03/11	23:57:00	39.50	76.40	3.1†		Fallston, Maryland
1906/05/08	17:41:00	38.7	75.7	3.0§	IV	Seaford, Delaware
1909/12/23	00:00:00	38.55	75.57	4.0‡		Seaford, Delaware
1937/12/03	17:15:00	38.68	75.38	2.8§	IV	Wood Branch, Delaware
1939/11/15	02:53:48	39.58	75.50	3.5‡		Salem, New Jersey
1964/05/12	06:45:10	40.30	76.41	3.8‡		Lebanon, Pennsylvania
1972/02/11	00:16:30	39.70	75.70	3.2§	V	Newark, Delaware
1972/12/08	03:00:33	40.14	76.24	3.3‡		Lititz, Pennsylvania
1973/02/28	08:21:32	39.72	75.44	3.8‖	V-VI	Wilmington, Delaware
1983/11/17	19:55:09	39.79	75.60	2.9‖	V	Wilmington, Delaware
1984/04/19	04:54:58	39.946	76.323	2.9‖	V	Lancaster, Pennsylvania
1984/04/23	01:36:02	39.946	76.323	4.1‖	V	Lancaster, Pennsylvania
1994/01/16	00:42:44	40.379	76.041	3.9#		Reading, Pennsylvania
1994/01/16	01:49:17	40.369	76.092	4.6#	VI	Reading, Pennsylvania
1997/11/14	03:44:11	40.164	76.276	3.0**		Lititz, Pennsylvania
2008/12/27	05:04:34	40.114	76.403	3.4**	IV	Akron, Pennsylvania
2009/07/01	13:44:43	39.644	75.483	2.8**		New Castle, Delaware
2017/11/30	21:47:31	39.198	75.433	4.2††	V	Dover, Delaware

*Maximum intensity in modified Mercalli intensity (MMI) scale.
†Location is the nearest town with the most felt reports.
‡Electric Power Research Institute (EPRI) (2012) catalog.
§Local magnitude assigned by Delaware Geological Survey.
‖$m_{b(Lg)}$ is the 1-s period *Lg*-wave magnitude of Nuttli (1973) reported in preliminary determination of epicenters, National Earthquake Information Center, U.S. Geological Survey.
#M_w is the moment magnitude, Du *et al.* (2003).
**M_L is the local magnitude for eastern North America, Kim (1998).
††M_w is the moment magnitude, this study.

throughout the New York–Philadelphia–Wilmington–Washington, D.C. urban corridor have felt small earthquakes and sustained damage from infrequent larger events since colonial times. New York City was damaged in 1737 and 1884 by earthquakes of magnitude ~5 (Sykes *et al.*, 2008). Moderately damaging earthquakes strike somewhere along the urban I-95 corridor roughly once every 50 yrs (Sykes *et al.*, 2008).

GROUND MOTION FROM THE MAINSHOCK

Regional *Lg* waves from the 2017 earthquake were observed with high signal-to-noise ratios at more than 380 broadband seismographic stations in the 70- to 2800-km epicentral distance range. We simulated high-frequency Wood–Anderson (W-A) records and measured the regional *Lg*-wave peak amplitude in the 0.8- to 10-Hz frequency band on vertical-component records recorded throughout the eastern United States and Canada. The peak amplitudes from the vertical W-A records from 381 broadband stations recording the 2017 Delaware earthquake are plotted against distance in Figure 2. The W-A peak amplitude decay with distance can be fit in the 70- to 2800-km distance range with the curve:

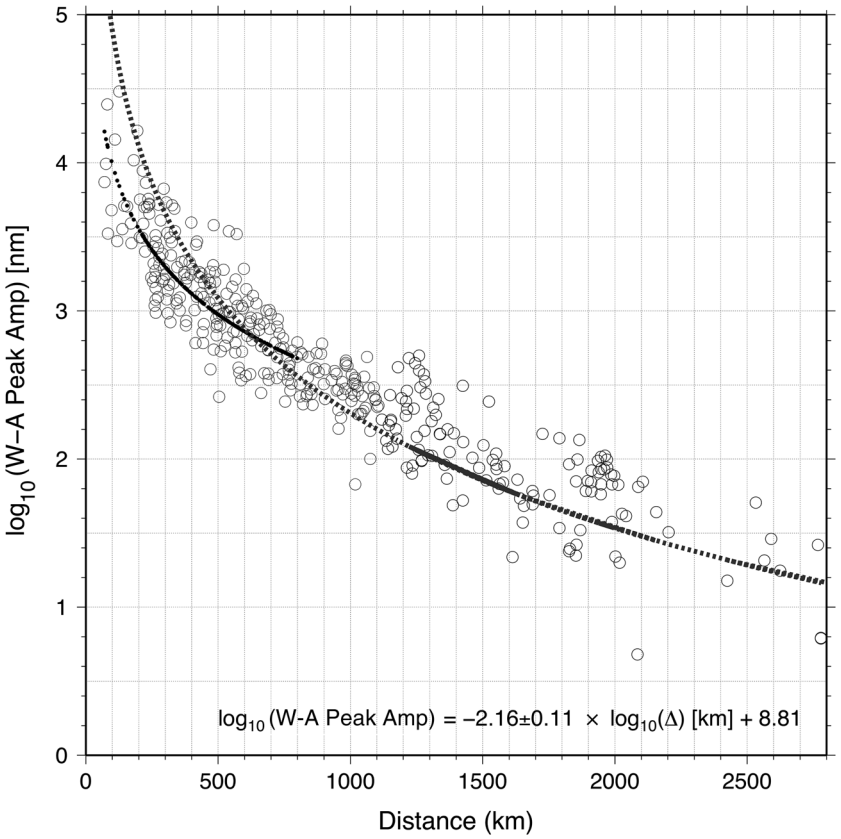

▲ **Figure 2.** 381 *Lg*-wave peak amplitudes measured on vertical Wood–Anderson (W-A) records from the 2017 Delaware earthquake are plotted against distance (circles). The W-A peak amplitude decay with distance can be fit with a curve: $\log_{10}(\mathrm{W-A\ peak\ amplitude}) = -2.16 \pm 0.11 \log_{10}(\Delta)(\mathrm{km}) + 8.81$. A dotted line represents amplitude–distance curve for the eastern North American local magnitude scale (Kim, 1998).

$$\log_{10}(\mathrm{W-A\ peak\ amplitude}) = -2.16 \pm 0.11 \log_{10}(\Delta)(\mathrm{km}) + 8.81.$$

This curve is obtained from a single event and is used here only as an illustration of data quality; nevertheless, it is comparable to known curves in eastern North America at distances up to 800 km (e.g., Kim, 1998) and provides a useful hint that the amplitude–distance curve for eastern U.S. earthquakes can be extended to 1500 km. High-frequency *Lg*-wave amplitude measurements at such long distances are remarkable. Observed *Lg*-wave peak amplitudes are plotted on geographic locations as circles that are color coded for their amplitude level in Ⓔ Figure S1 (available in the electronic supplement to this article).

The ground motions from the 2017 Delaware earthquake, such as those from the 2011 Mineral, Virginia, earthquake, demonstrate the low-seismic attenuation of crustal rocks in eastern North America compared with those in western North America; the geologically old crystalline rocks of central and eastern North America extend levels of ground motion to much greater distances than in the geologically young western North America (e.g., Nuttli, 1973; Frankel *et al.*, 1990; McNamara *et al.*, 2014; Bockholt *et al.*, 2015). The wide extent of the felt area for the Dover earthquake and the relatively high peak amplitudes at large distances are consistent with this low attenuation, which has important implications for the extent of damage during earthquakes (e.g., Pratt *et al.*, 2017).

ShakeMap and Community Internet Intensity Map

The ShakeMap of instrumental intensity for the 2017 Delaware earthquake is generated using ground-motion observations at permanent seismographic stations around the epicenter (see Data and Resources). ShakeMap is useful for postearthquake emergency management and earthquake loss mitigation. The closest station is GEDE ($\Delta = 69$ km, Az = 347°) followed by WUPA ($\Delta = 82$ km, Az = 351°) and others. These stations recorded only weak ground motions, so the ShakeMap generated using data from these stations was augmented by intensity observations reported via the USGS DYFI system. We generated a CIIM that includes geocoded Community Decimal Intensity (CDI) aggregated data (Dengler and Dewey, 1998) from the USGS DYFI (see Data and Resources and Fig. 3). Reports including an address are grouped together in 10-km squares, and the CDI is calculated from the community internet intensity weighted sum of averages of those reports. The ground velocity measurements at seismographic stations in the region are converted to corresponding MMI values based on the Worden *et al.* (2012) relation as shown in Ⓔ Figure S2. The ShakeMap for the 2017 Delaware earthquake appears less informative in terms of ground shaking from the mainshock than the CIIM generated from a total of 16,290 responses (6584 responses in the first 52 min after the shock) with the maximum felt report of V (MMI).

Regression of 23 peak ground velocity measurements for the 2017 Delaware earthquake and corresponding MMI values indicates that neither the Worden *et al.* (2012) relation for California nor the Atkinson and Kaka (2007) relationships between felt intensity and instrumental ground motion for central United States (CUS) are consistent with 2017 Delaware ground motion. We obtained relationships between felt intensity and instrumental ground motion for the mid-Atlantic region as

$$\mathrm{MMI} = 3.3 \log_{10}(\mathrm{peak\ velocity})(\mathrm{cm/s}) + 9.9.$$

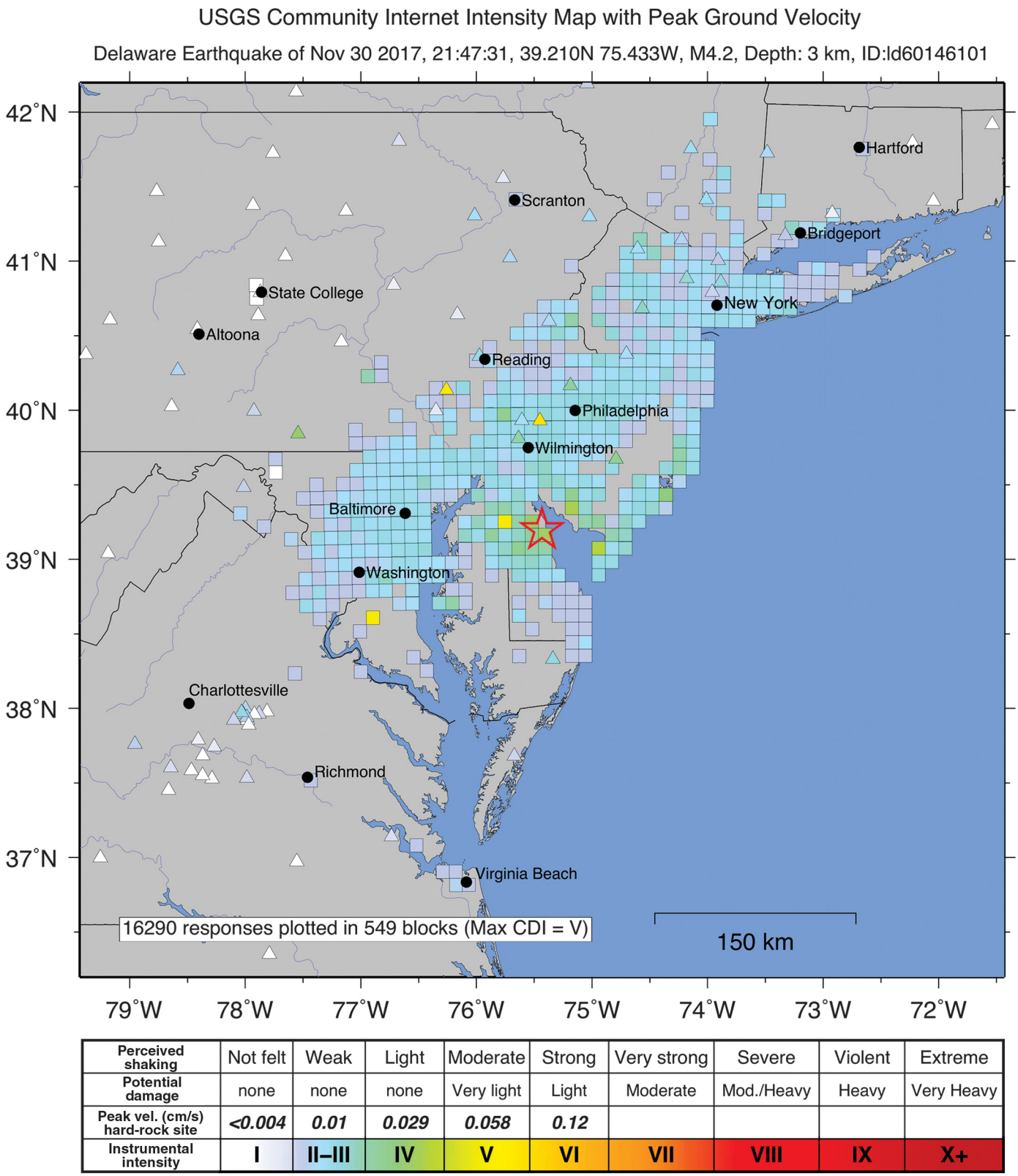

Perceived shaking	Not felt	Weak	Light	Moderate	Strong	Very strong	Severe	Violent	Extreme
Potential damage	none	none	none	Very light	Light	Moderate	Mod./Heavy	Heavy	Very Heavy
Peak vel. (cm/s) hard-rock site	*<0.004*	*0.01*	*0.029*	*0.058*	*0.12*				
Instrumental intensity	I	II–III	IV	V	VI	VII	VIII	IX	X+

▲ **Figure 3.** The Community Internet Intensity Map generated using geocoded Community Decimal Intensity (CDI) aggregated data from the U.S. Geological Survey (USGS) Did You Feel It? (DYFI) system. The felt reports submitted online are assigned modified Mercalli intensity (MMI) numbers and are grouped together in 10-km squares. Intensity values for seismic stations are determined from their peak ground velocity in cm/s as shown in the legend. The color scale for this map is shifted compared with the default used in ShakeMap to emphasize MMI within the II–V range for this moderate-size shock with the peak CDI = V.

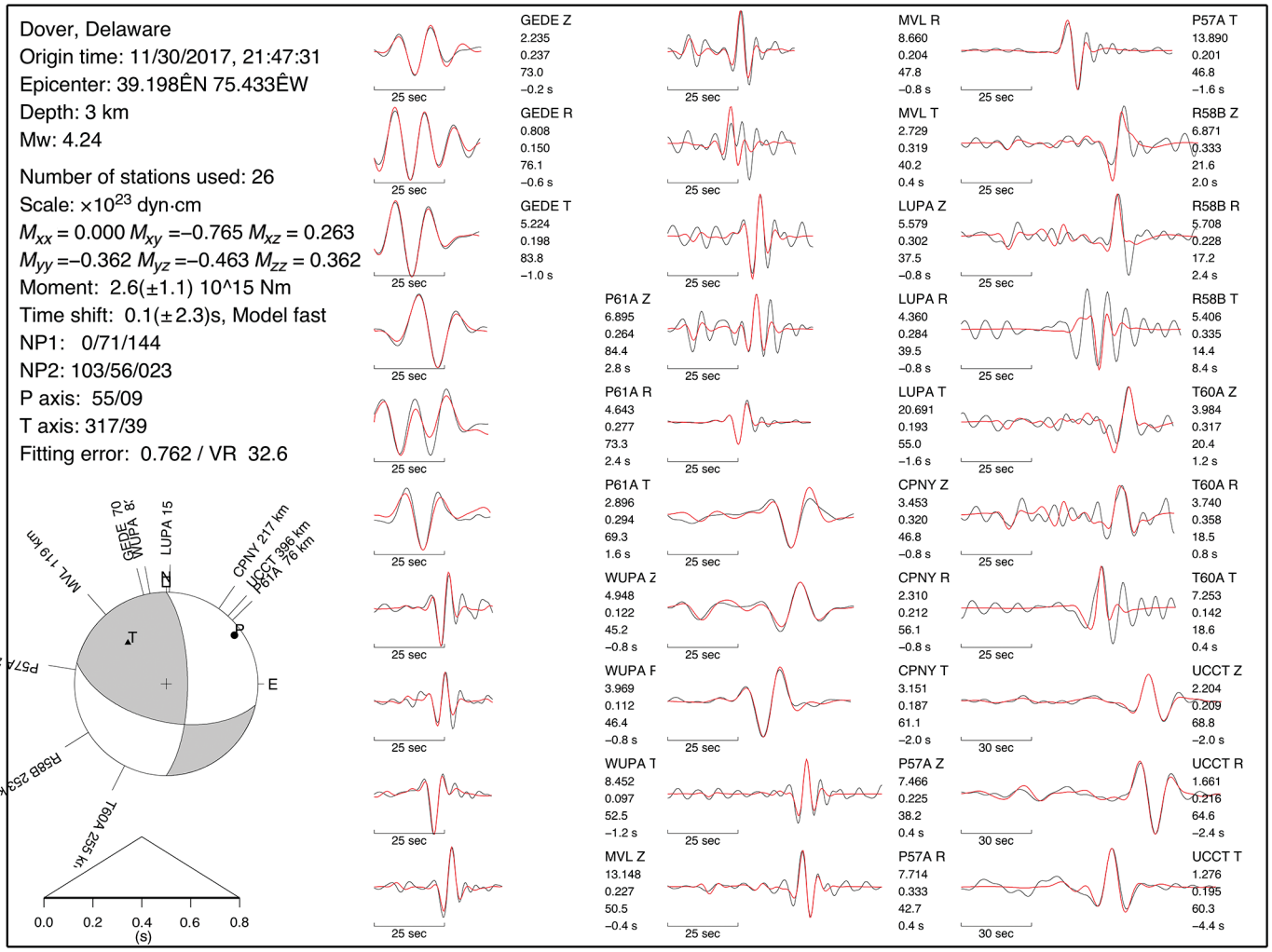

▲ **Figure 4.** Comparison between observed (black lines) and synthetic (red lines) waveforms of the 30 November 2017 earthquake. Synthetic seismograms are calculated for a focal depth of 3 km, and only 30 of 78 traces used are shown. Station code and component (Z, vertical; R, radial; and T, transverse components), peak amplitude of the observed signal in micrometers, seismic moment in 10^{15} N · m, variance reduction in percentage, and time shift Δt in seconds are indicated at the end of each trace. Focal mechanism of the event is represented by the typical focal mechanism plot representation of lower-hemisphere projection. Shaded quadrants denote compressional motion for *P* waves. The epicentral distance of each station is marked around the focal mechanism plot according to azimuth. For stations whose *P*-wave polarity data are used, a circle is plotted for compressional first motion, and a triangle is used for dilatational first motion. Two nodal planes (NP1 and NP2) as well as azimuth and plunge angle in degrees of the P and T axes are indicated. A simple triangular source time function used is shown at the lower left.

The intensities for seismic stations are determined by peak ground velocity as shown in the map legend (Fig. 3). The color scale for this map is shifted compared with the default used in CIIM to emphasize MMI within the II–V range for the 2017 Delaware earthquake. This relation is based only on data from the Delaware earthquake and requires thorough analysis of all significant earthquakes with sufficient intensity reports. This exercise suggests that known relationships between felt intensity and instrumental ground motion for California (e.g., Worden *et al.*, 2012) or CEUS (e.g., Atkinson and Kaka, 2007) are not adequate for the mid-Atlantic coastal region.

FOCAL MECHANISM AND DEPTH OF THE MAINSHOCK FROM REGIONAL WAVEFORM INVERSION

The earthquake on 30 November 2017 was recorded well enough for its seismic moment, focal mechanism, and focal depth to be determined by modeling observed seismic records at permanent seismographic stations around the study area (Fig. 4). We used a regional waveform inversion method described by Kim and Chapman (2005) using a grid-search inversion technique over strike (θ), dip (δ), and rake (λ) developed by Zhao and Helmberger (1994). A CUS crustal

Table 2
List of Earthquakes That Occurred Close to 30 November 2017 Delaware Earthquake

ID	Date (yyyy/mm/dd)	Time (hh:mm:ss.s)	Latitude (°N)	Longitude (°W)	*h* (km)	Magnitude (M_L)	*N*	Gap (°)	*Dh* (km)	CC1	CC2
01	2010/09/16	16:06:20.1	39.2359	75.4404	3.8	2.1	25	203	3.21		1.00
02	2010/10/26	22:30:03.9	39.2431	75.5071	5.0	1.4	8	277	5.88		0.67
03	2015/10/07	08:44:21.9	39.2110	75.4149	5.9	1.7	17	143	1.70		0.84
04	2017/11/20	14:24:48.4	39.2249	75.4422	3.0	1.5	16	232	5.90	0.58	0.36
05	2017/11/30	21:47:30.2	39.2066	75.4426	4.7	4.2	41	127	1.32		0.35
06	2017/12/01	05:37:34.0	39.1794	75.4240	6.0	1.3	8	328	2.83	0.41	0.20
07	2017/12/11	22:02:40.2	39.2168	75.3874	4.4	1.3	9	271	3.66	0.79	0.33
08	2017/12/13	00:45:26.0	39.2539	75.4537	4.0	1.6	11	252	3.50	0.90	0.49
09	2017/12/17	14:58:44.4	39.2345	75.4638	4.0	1.9	16	253	2.50	1.00	0.63
10	2017/12/17	16:07:05.4	39.2212	75.4255	3.5	1.5	12	255	7.22	0.42	
11	2017/12/23	16:21:50.8	39.1792	75.3267	3.0	0.9	8	107	1.42	0.22	
12	2017/12/31	00:11:19.8	39.1756	75.4013	2.5	0.9	14	162	3.24	0.50	
13	2018/02/02	08:57:47.6	39.2274	75.4113	4.0	1.4	10	282	5.88	0.50	0.25

Gap, seismographic station coverage gap in location; *h*, focal depth in kilometers, depth is fixed in location for events: 4, 8, 9, and 13; *Dh*, horizontal location error in kilometers (semimajor axis of error ellipse in 95% confidence level); CC1, correlation score of GEDE records of each event; CC2, correlation score of MVL records of each event using 1 as template event; location for two small events—11 and 12—is that of the template event (9).

model with three layers over a half-space and a 1-km-thick surface low-velocity layer was used (Herrmann, 1979; Du *et al.*, 2003). The focal mechanism of the mainshock on 30 November 2017 indicates predominantly strike-slip faulting with significant oblique thrust motion (~25%). The focal mechanism suggests a north–south-striking ($\theta = 0°$) nodal plane steeply dipping to the east ($\delta = 71°$) and a second nodal plane striking nearly east–west ($\theta = 103°$) and moderately dipping south ($\delta = 56°$). The focal depth is constrained to be about 3 km with a seismic moment $M_0 = 2.6 \pm 1.1 \times 10^{15}$ N · m, which corresponds to a moment magnitude $M_w = 4.24$ (see Fig. 4). The best-fitting double-couple source mechanism parameters are $\theta = 0°$, $\delta = 71°$, and $\lambda = 144°$ (second nodal plane; $\theta = 103°$, $\delta = 56°$, and $\lambda = 23°$). The subhorizontal P axis trends southwest–northeast (55°) with a plunge of 9°, and the T axis trends northwest–southeast (317°) with a plunge of 39°. The P-axis orientation is similar to that of the 16 January 1994 earthquake in Reading, Pennsylvania (61°), which is the nearest earthquake with a known focal mechanism (Du *et al.*, 2003). Comparison between synthetic and observed waveforms indicates that a focal depth of 3 ± 1 km best fits observations.

The National Earthquake Information Center (NEIC) of the USGS reported moment tensor solution with a moment magnitude $M_w = 4.1$ and comparable focal mechanism with fault parameters: strike = 106°, dip = 62°, and rake = 40° (see Data and Resources). Saint Louis University (SLU) published a similar solution with $M_w = 4.18$, and strike = 100°, dip = 60°, and rake = 25° (see Data and Resources). All three known moment tensor solutions, including this study, indicate a focal depth of 3 km. However, the moment tensor solutions of SLU and this study indicate a strike-slip stress regime, but the NEIC solution suggests an oblique thrust faulting with a transpressional stress regime.

The locations of aftershocks discussed in the next section have relatively large location uncertainties. However, relocations of the mainshock and its aftershocks discussed in the Relocation of the 2017 Delaware Earthquake Sequence: Preliminary Result section suggest that the relocated aftershocks align west-northwest–east-southeast and that the nodal plane striking east–west ($\theta = 103°$) is the likely fault plane for the mainshock (see Fig. 1).

DETECTION AND LOCATION OF AFTERSHOCKS AND FORESHOCKS

The regional permanent seismographic stations of LCSN detected two aftershocks that occurred close to the mainshock: a magnitude 1.6 event on 13 December 2017 and a magnitude 1.9 event on 17 December 2017 (Table 2). No felt earthquake or events greater than magnitude 2.0 have occurred in the region since the mainshock. To search for any low-magnitude aftershocks, we applied a waveform cross-correlation detector using the permanent regional station data (e.g., Schaff, 2008; Kim, 2013).

The waveform correlation detector is known to lower the seismic event detection threshold by about 1.0 magnitude unit beyond what is normally detected through standard processing (e.g., Gibbons and Ringdal, 2006; Kim and Kim, 2014, among others). We used three-component records at the two nearest stations, GEDE ($\Delta = 69$ km, Az = 347°) and WUPA ($\Delta = 82$ km, Az = 351°), from the aftershock

on 17 December 2017 at 14:58 (event 9) as a template event to detect additional small aftershocks. The three-component template waveforms are 21 s long for GEDE and 28 s long for WUPA. Template traces start about 1 s before the *P* arrival and extend 12 and 18 s after *S* arrivals for GEDE and WUPA, respectively. GEDE template traces are a few seconds shorter than those of WUPA because of local quarry blast signals closely following the *Lg*-wave coda. The records are filtered between 2 and 8 Hz to improve signal-to-noise ratios. Large signal durations (T) and wide-frequency bandwidths (B) are the key for a robust correlation detector. Harris (1991) suggested that a time–bandwidth product ($T \times B$) exceeding 100 (or smaller $T \times B$ with more stations) is necessary for reliable event attribution. We find that the 21 s for GEDE and 28 s for WUPA window lengths yield time–bandwidth products large enough to enable reliable detections. We take the mean of the cross-correlation scores from the three components to enhance the robustness of event detection. The local magnitude (M_L) of the earthquakes we identified with the correlation detector in the Dover, Delaware, area were determined from the root mean square (rms) amplitudes of detected signals in the time windows and calibrated to the amplitudes of the template traces with known magnitude.

We used a correlation detection threshold at 0.2 and 0.3 for GEDE and WUPA, respectively. The threshold values are based on noise correlation using a time-reversed template as reported by Slinkard *et al.* (2014). Time reversing the template ensures the new template has the same time–bandwidth product as the original template and should yield a very similar distribution of correlation values in the noise window. The distributions only varied at high values because only the forward templates generate high correlation values from correlations with similar waveforms. The 17 December 2017 14:58 (event 9) time-reversed template yields the maximum correlation values of 0.182 and 0.303 for GEDE and WUPA, respectively. We set these values as false detection threshold for each three-component template.

We detected 10 events using the 17 December 2017 14:58 GEDE three-component templates with a threshold of 0.2. The WUPA three-component templates detected 19 events that exceed the threshold of 0.3 from 1 December 2017 through 1 March 2018. We select events by associating detection time at two stations such that GEDE and WUPA detection times are within 2.5 s. We found eight common detections from the two stations that show correlation scores between 0.25 and 1.0 and magnitudes between 0.9 and 1.9 (magnitude of the template event). Examination of waveform data of detected events indicates that seven events can be located using regional stations. Vertical-component records from these earthquakes recorded at GEDE ($\Delta \sim 69$ km) are plotted in Figure 5. The events together with their location error ellipses are listed in Table 2. We searched for possible small foreshocks before the mainshock on 30 November 2017 using the 17 December 2017 14:58 event templates at GEDE and WUPA for three months, September–November 2017. We detected a single foreshock on 20 November 2017 at 14:24:47 with an average three-component correlation score of 0.61 at GEDE and WUPA with a magnitude of 1.5 (see Table 2).

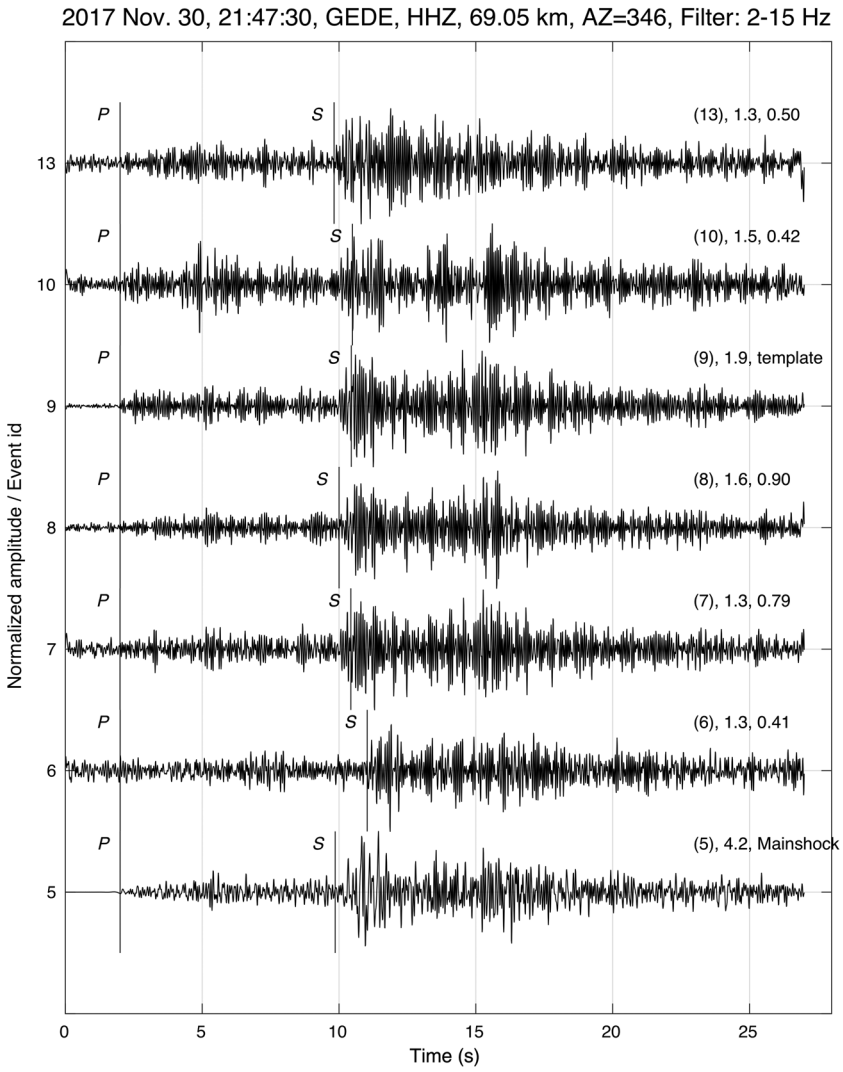

▲ **Figure 5.** Vertical records at GEDE from the mainshock (event 2) and six aftershocks are plotted for 2 s before *P* arrival and 17 s after the *P* arrival. Event ID, local magnitude, and cross-correlation score are indicated at the end of each trace. See Table 2 for details.

Detection of Repeating Earthquakes

Comparison of waveforms recorded by LCSN for the 2017 Dover earthquake against unclassified seismic event files in the LCSN seismic database allowed us to identify a magnitude

M_L 2.1 earthquake. The event on 16 September 2010 at 16:06 was initially poorly located by LCSN (see Table 2), but reexamination of its waveform records revealed that it must have occurred close to the location of the 2017 Delaware mainshock. We searched event files from the past 7 yrs, between September 2010 and October 2017, using three-component correlation detectors for additional small earthquakes that may have occurred around the location of the 2017 Delaware earthquake.

We detected two small earthquakes, the first one on 26 October 2010 at 20:30 (M_L 1.4) and the second event on 7 October 2015 at 08:44 (M_L 1.7), using the multichannel correlation detector on three-component, continuous waveform data at close stations: PSUB ($\Delta = 77$ km, Az = 0°), MVL ($\Delta = 115$ km, Az = 318°), and SDMD ($\Delta = 122$ km, Az = 280°). Based on their waveform similarity, these two newly detected earthquakes as well as the events on 16 September 2010, 17 December 2017, and the mainshock on 30 November 2017 must have occurred close to the first event on 16 September 2010, which was used as the template event (see Table 2). Waveform similarity of three events, 16 September 2010, 7 October 2015, and 17 December 2017, recorded at MVL plotted in Figure 6, suggests that these events may be considered repeating earthquakes occurring with relatively large time intervals—5 yrs between the 2010 and 2015 events and 2.2 yrs from the 2015 and 2017 events.

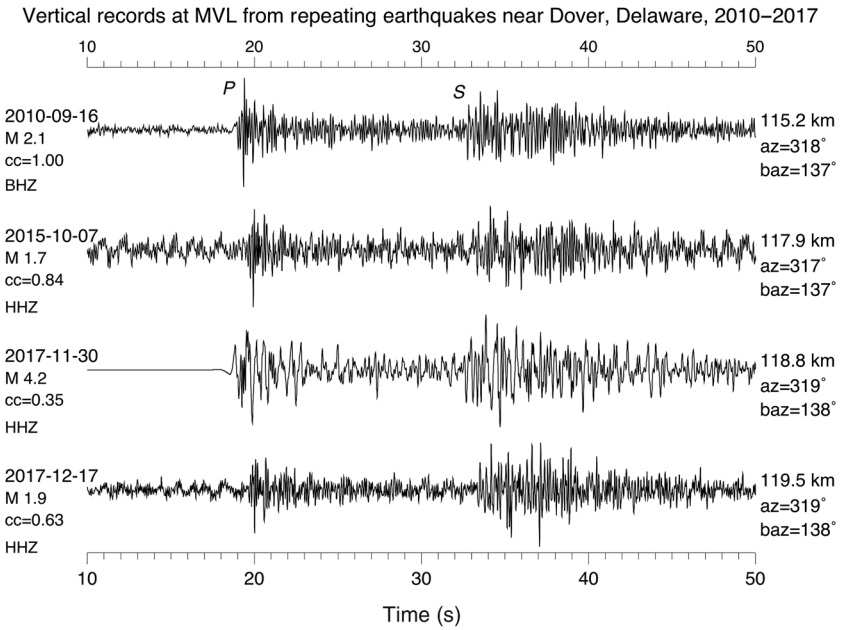

▲ **Figure 6.** Vertical records at MVL (Millersville University, Pennsylvania) from four selected repeating earthquakes near Dover, Delaware, during September 2010 and December 2017. The first known event on 16 September 2010 (M_L 2.1, top trace) is used as the template event. About 25-s-long records starting from 1 s before *P* arrival to 10 s after *S* arrival are used to detect small events using waveform cross-correlation detector. All three-component records are simultaneously examined with an average cross-correlation coefficient of 0.27 as detection threshold based on the reversed-time template. Event date, magnitude, cross-correlation coefficient, and channel ID are indicated at the beginning of each trace.

Aftershock Location and Location Accuracy

Between September 2017 and February 2018, a foreshock (M_L 1.5) and eight small aftershocks (M_L 0.9–1.9) were detected around the mainshock epicenter. These earthquakes were located using *P* and *S* arrival times at regional stations. The locations of these earthquakes were not accurate because of sparse seismic station coverage (Fig. 1).

Six aftershocks with $M_L \geq 0.9$ (Table 2) occurring in the area of the mainshock between 30 November 2017 and February 2018 were located using HYPOINVERSE (Klein, 2007). The velocity model used for location is an average 1D model for the CUS consisting of a 1-km top layer with *P*-wave velocity of 5.0 km/s and a 9-km-thick upper-crustal layer with *P*-wave velocity of 6.1 km/s (Herrmann, 1979). The *S*-wave velocities are set at $V_P/\sqrt{3}$. All events were located with *P*- and *S*-wave arrival times from at least six seismographic stations in and around Delaware. For the six earthquakes between November 2017 and February 2018, the nearest station is at ~65 km distance, but most stations were at 100- to 150-km distances with an azimuthal gap of about 250° (Fig. 1 and Table 2). For most of these aftershocks, we fixed the depth at 3 or 4 km to improve location stability. The location uncertainties are large—horizontal errors are up to 7.2 km for the 95% confidence level as listed in Table 2. The locations of eight aftershocks, a foreshock, and three repeating events during 2010–2015 with their horizontal error ellipses are plotted in Figure 7.

LOCAL PORTABLE SEISMOGRAPHIC NETWORK DEPLOYMENT

The 2017 Delaware earthquake led to a rapid deployment of instruments to record aftershocks. Personnel from the LDEO, the Department of Terrestrial Magnetism of the Carnegie Institution for Science, the University of Maryland, Lehigh University, and the USGS mobilized the day after the earthquake to install 18 instruments in the epicentral area using a mix of instruments. The earthquake provided the opportunity to test our ability to rapidly deploy instrumentation in the mid-Atlantic region of the United States after earthquakes and to collaborate on studies of the data collected from aftershock deployments. These five groups rapidly organized during the evening after the earthquake to coordinate the deployment of an array of seismic instruments, 10 high-frequency nodal seismographs (University of Maryland), 4 broadband (Carnegie), and 4 short- and medium-period stations (Lamont). Coordination was facilitated by individuals who knew each other and were able to rapidly self-organize the deployment.

The aftershock response team from the Department of Geology, University of Maryland, College Park, and the USGS

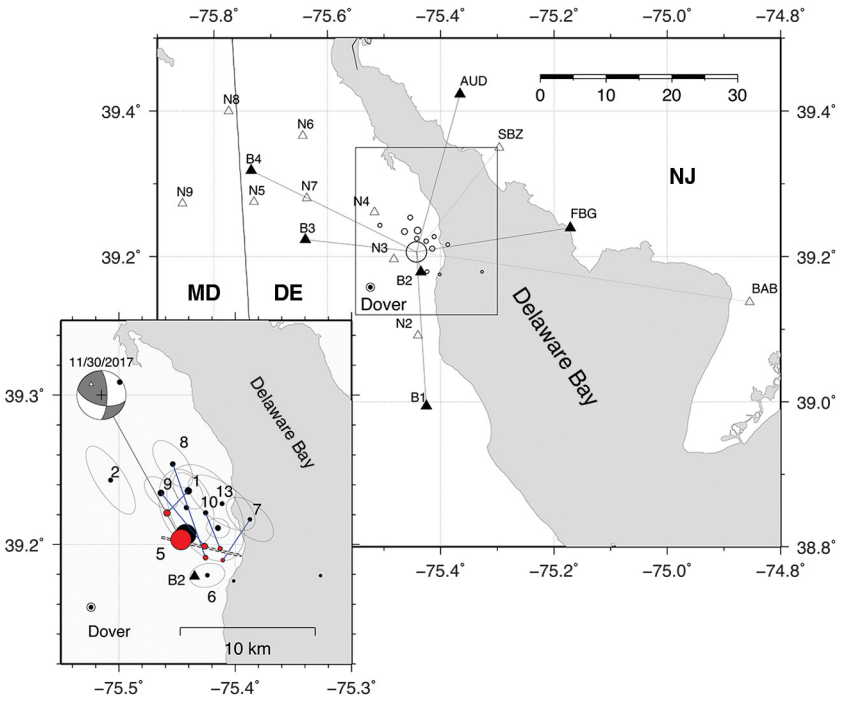

▲ **Figure 7.** Local portable seismographic stations deployed on 1 December 2017 after the Delaware earthquake on 30 November 2017. Stations with broadband sensors are plotted by solid triangles, and short-period sensors are plotted by open triangles. Events detected and located by regional stations are plotted by open circles. Stations used for relocations are indicated by lines connecting to the mainshock. (Inset) Single-event locations of the 13 regional earthquakes that occurred and located near Dover, Delaware, from September 2010 through February 2018 are plotted with black circles. The horizontal location uncertainties are represented by 95% confidence error ellipses given in Table 2. Six relocated events are plotted by red circles, and their initial locations are connected by blue lines to indicate improvements in relocation. Strike of the east–west-trending nodal plane is indicated by dashed line. Mainshock and its four aftershocks align west-northwest–east-southeast—coinciding with strike of a nodal plane of the mainshock focal mechanism.

deployed 10 FairfieldNodal ZLand nodes containing three-component 5-Hz geophones. The compact waterproof units contain sensors, batteries, digitizers, recorders, and Global Positioning System antennas that can obtain location and timing information even through a few centimeters of overlying soil. Two teams deployed a total of 10 nodes by burying them directly into 20- to 30-cm-deep holes. Despite very cold temperatures, self-contained batteries powered the nodes to record ground motions at 4 ms sampling for 37–40 days.

The aftershock response team from the Department of Terrestrial Magnetism of the Carnegie Institution for Science deployed four Nanometrics Trillium 120 Compact Posthole broadband seismometers. These sensors are waterproof and designed for direct burial, so they were deployed directly into holes approximately 60–90 cm deep, oriented and leveled, while surrounding soil and clay was used to bury them. This deployment was used as a test run for the recently developed Carnegie Quick Deploy Box (Roman *et al.*, 2017) that provides a single-box, grab-and-go system for the rapid installation of broadband seismic stations. All four sites used solar power and ran uninterrupted from 1 December 2017 until 11 January 2018.

The aftershock response team from LCSN (Lamont and Lehigh) deployed four temporary stations along the northern shore of Delaware Bay and the southern coast of New Jersey. Two short-period ($T_0 = 2$ Hz) and two medium-band seismometers ($T_0 = 30$ s) were placed on paving stones in shallow holes dug in unconsolidated soil. One site operated on solar power and battery, and the other three stations were on AC power supply backed up by battery. The deployment lasted from 1 December 2017 to 11 January 2018 (see Data and Resources).

Local portable seismographic stations deployed on 1 December 2017 after the Delaware earthquake on 30 November 2017 are plotted in Figure 7. Stations with broadband sensors are plotted by solid triangles; short-period sensors (including nodals) are plotted by open triangles. Epicenters of events detected and located by regional stations are plotted by open circles, including small aftershocks of the 2017 Delaware earthquake sequence.

Relocation of 2017 Delaware Earthquake Sequence: Preliminary Result

Seven events of the 2017 Delaware earthquake sequence (events 5–10; Table 2) and event 1 on 16 September 2010 were relocated using the double-difference earthquake relocation algorithm (Waldhauser and Ellsworth, 2002) to identify the fault plane from two nodal planes of mainshock focal mechanism (Fig. 4). We used differential travel-time data of event pairs derived from the *P*- and *S*-wave arrival times used in location to determine precise relative locations for these earthquakes. We used the computer program hypoDD, which uses the double-difference algorithm (Waldhauser, 2001). We obtained 75 *P*-wave and 76 *S*-wave differential travel times from the phase pick data using the event pairs with separation distances of up to 5 km.

The waveform cross-correlation method is used to improve the precision of the differential travel-time measurements and the cross-correlation data are combined with the phase pick data. We used a 1.0- to 1.5-s-long window centered at the *P*-arrival time on vertical records, and a 1.5- to 2.5-s-long window around the *S* arrival on north–south-component records for waveform cross correlation. We obtained 28 *P*-wave differential times and 78 *S*-wave differential times from waveform cross correlation with correlation coefficients greater than 0.70. For four events (events 7–10) that occurred during 11–17 December 2017, waveform data from the eight temporary stations deployed on 1 December 2017 are used for this preliminary relocation. Stations used are indicated in Figure 7.

We attempted to relocate seven events, although event 6 was not relocated because of large rms residual. The five relocated events—mainshock and its four aftershocks—aligned linearly along a plane trending ~105° and extending about 3 km (Fig. 7), which is nearly parallel with the orientation of the west-northwest–east-southeast-striking nodal plane (strike = 103°) of the double-couple focal mechanism (Fig. 4). All six relocated earthquakes are at depth 3 ± 1.2 km. Relocations show a focusing of the events into a tighter cluster close to the mainshock (Fig. 7).

DISCUSSION

Repeating Earthquakes

We detected four small repeating earthquakes spread in time up to 5 yrs apart at the northeastern tip of the Delmarva Peninsula in a typical stable continental margin setting. All detected events must be repeating events clustered within less than a few kilometers from each other based on their waveform similarity represented by three-component waveforms with high cross-correlation coefficients (Table 2, and Figs. 5 and 6). The waveform cross-correlation-based detector provided identification of small repeating earthquakes on an expanded time window. This may suggest the existence of repeating earthquakes even in stable regions with relatively low seismicity (e.g., Schaff and Richards, 2011; Kim and Kim, 2014).

We cannot say whether additional small earthquakes occurred in the Dover, Delaware, area before 2010 because high-quality continuous waveform data from permanent stations in the region were unavailable before 2010, and close-in stations were lacking. The smallest event detected using the three nearest stations is an M_L 1.4 event (event 2, Table 2), and we estimate the magnitude detection threshold from 2010 to 2017 for the Dover, Delaware, area to be about M_L 2.0. Hence, our detection of small shocks in the region is likely incomplete because of a lack of close stations.

Focal Mechanism and Regional Variation of *P*-Axis Orientation

The moment tensor inversion for the 30 November 2017 Delaware earthquake using regional long-period waveforms indicates that the focal mechanism is predominantly strike-slip faulting with a significant thrust faulting component (Fig. 4). Whereas the subhorizontal P-axis plunges 9° and trends southwest–northeast (55°), the T axis trends northwest–southeast (317°) with a plunge of 39°. This P-axis orientation is similar to that of the 16 January 1994 earthquake in Reading, Pennsylvania, whose subhorizontal P-axis plunges about 2° and trends east-northeast (61°), which is the nearest earthquake with a known focal mechanism (Du *et al.*, 2003). The focal mechanism of the 2011 M_w 5.8 Mineral, Virginia, earthquake, 270 km southwest of the 2017 Delaware earthquake, showed nearly pure thrust faulting with subhorizontal P axis plunging ~4° and trending 103° and near-vertical T axis (plunge = 82°) trending 42° (Chapman, 2013; McNamara *et al.*, 2014). The P-axis azimuth around the 2017 Delaware earthquake is rotated about 45° from that in central Virginia. This difference may be due to the fact that the epicentral area of the Dover earthquake is at the northern edge of a transition zone with regard to the strike of geologic structures in the eastern United States (Horton *et al.*, 1991). To the south of the transition zone, geologic boundaries of Paleozoic units and associated faults trend about N40°E–N50°E throughout the Maryland and Virginia Piedmont near the epicenter of the 2011 earthquake, as do the trends of a steep gradient in crustal thickness (Soto-Cordero *et al.*, 2018) and Mesozoic rift basins. Starting in Maryland just south of the epicentral area, units turn more to the east to have a N55°E–N65°E trend within the epicentral region and eastern Pennsylvania, but they eventually change direction farther north back to a northeast trend again. The variation of P-axis orientation and the possibly related changes in strike of geologic structure from north to south along the Atlantic coastal region indicate complexity in the stress field both today and in the past.

The Importance of High-Quality Monitoring Networks and Rapid Response Capabilities

The assessment of seismic hazard in low-strain continental margin settings such as the eastern United States is particularly challenging. In the past 150 yrs, the U.S. mid-Atlantic region has experienced multiple earthquakes with magnitudes as high as M_w 4.6–5.8, and the eastern North American seaboard has experienced earthquakes up to M_w 7.3 (e.g., 1929 M_w 7.2 Grand Banks, 1933 M_w 7.3 Baffin Bay earthquakes, and M_w 7.3 Charleston earthquakes). Given the major population centers, large stock of unreinforced masonry structures, critical infrastructure, commercial and industrial development, and concentration of governmental and financial institutions located in the I-95 mid-Atlantic corridor, the occurrence of a large earthquake on the East Coast represents a high-risk event that could result in substantial direct and indirect economic losses. Soto-Cordero *et al.* (2018) documented statistically significant spatially clustered seismicity extending from central Virginia through Maryland, Pennsylvania, New York, and into New England. These types of analyses are limited by observational capabilities that do not fully capture seismicity in the eastern United States. Recent investment in earthquake monitoring networks and the ability to rapidly respond to seismic events with dense focused temporary deployments in the CEUS provide critical data to better define earthquake source regions and to assess earthquake hazards.

CONCLUSIONS

The 30 November 2017 Delaware earthquake with magnitude M_w 4.2 is the largest instrumentally recorded earthquake in Delaware. It occurred at a shallow depth of 3 km along an east–west-trending fault beneath the northeastern tip of the Delmarva Peninsula near Dover, Delaware. The earthquake and its aftershocks provide an opportunity to evaluate seismicity in a passive margin setting using much improved coverage by high-quality permanent broadband seismographs at regional distance ranges in the CEUS. High-quality seismic recordings at over 380 permanent regional broadband seismographic stations in the eastern United States show a remarkably small decrease in amplitude with distance between 800 and 2000 km.

The mainshock focal mechanism shows predominantly strike slip with a significant thrust component. The orientation of the subhorizontal P axis is consistent with that of earthquakes in the nearby Reading-Lancaster seismic zone in Pennsylvania but are rotated counterclockwise about 45° from that of the 2011 M_w 5.8 Mineral, Virginia, earthquake.

We detected small earthquakes below the normal event detection threshold using a waveform cross-correlation detection method. Based on the waveform similarities, those events detected in 2010, 2015, and 2017 are considered repeating earthquakes. Although there is a large time interval between events, these events occurred within a spatially tight cluster located near the 2017 Dover, Delaware, earthquake. This demonstrated the effectiveness of this approach for earthquake studies and hazard evaluation in the eastern United States.

DATA AND RESOURCES

The other data are derived from the following sources: Earthquake catalog for Delaware since 1871 at http://www.dgs.udel.edu/delaware-geology/catalog-delaware-earthquakes-spreadsheet (last accessed July 2018); northeastern U.S. earthquake catalog from Lamont Cooperative Seismographic Network (LCSN) at http://billie.ldeo.columbia.edu:8080/data.search.html (last accessed July 2018); Advanced National Seismic System (ANSS), Comprehensive Catalog (ComCat) at https://earthquake.usgs.gov/earthquakes/search/ (last accessed July 2018); waveform data from the aftershock monitoring deployment archived at Incorporated Research Institutions for Seismology Data Management Center (IRIS-DMC) Network code: Y3 (Delaware 2017 aftershock study) at http://ds.iris.edu/SeismiQuery/by_network.html (last accessed July 2018); waveform data from the aftershock monitoring deployment: description at doi: 10.7914/SN/Y3_2017; waveform data from LCSN, N4, and other networks in the central and eastern United States (CEUS) at http://ds.iris.edu/SeismiQuery/by_network.html (last accessed July 2018) and http://ds.iris.edu/ds/nodes/dmc/forms/breqfast-request/ (last accessed July 2018); U.S. Geological Survey (USGS) Community Internet Intensity Map at https://earthquake.usgs.gov/earthquakes/eventpage/us1000bjkn#dyfi (last accessed July 2018) "Did You Feel It?" (DYFI) at https://earthquake.usgs.gov/data/dyfi/ (last accessed July 2018); USGS ShakeMap at https://earthquake.usgs.gov/earthquakes/eventpage/us1000bjkn#shakemap (last accessed July 2018); LCSN ShakeMap at http://nyack.ldeo.columbia.edu/shake/60146101/products.html (last accessed July 2018); regional moment tensor solutions National Earthquake Information Center (NEIC)/USGS at https://earthquake.usgs.gov/earthquakes/eventpage/us1000bjkn#moment-tensor (last accessed July 2018); and Saint Louis University at http://www.eas.slu.edu/eqc/eqc_mt/MECH.NA/20171130214731/index.html (last accessed July 2018).

ACKNOWLEDGMENTS

The authors thank two reviewers whose comments help clarify certain issues in the original article. The temporary Dover, Delaware, network could not have been deployed without the help of volunteers. The authors thank Erin Cunningham, Chao Gao, Quancheng Huang, and Peter Meehan from the University of Maryland; Helen Janiszewski and Steven Golden from the Carnegie Institution for Science; Adrienne Scott, Anne Sirait, and Krittanon Sirorattanakul from Lehigh University; Lisa Schleicher from the Defense Nuclear Facilities Safety Board; Craig Rhodes and Bill Jones of the Milford Neck Wildlife Refuge, Officer Dool of the Delaware Division of Fish and Wildlife in the Delaware Department of Natural Resources and Environmental Control; and the many private landowners who allowed us to install seismic stations on their properties. Vedran Lekic acknowledges support from the Packard Foundation. This study is partially supported by the U.S. Geological Survey Cooperative Agreement for Seismic Network Operations under Cooperative Agreement G15AC00045 to Lamont–Doherty Earth Observatory. This is Lamont–Doherty Earth Observatory Contribution Number 8248.

REFERENCES

Armbruster, J. G., and L. Seeber (1987). The April 23, 1984, earthquake and the Lancaster seismic zone in eastern Pennsylvania, *Bull. Seismol. Soc. Am* **77,** 877–887.

Atkinson, G., and S. Kaka (2007). Relationships between felt intensity and instrumental ground motions for earthquakes in the central United States and California, *Bull. Seismol. Soc. Am.* **97,** 497–510.

Baxter, S. J. (2000). Catalog of earthquakes in Delaware, *Open-File Rept. No. 42*, Delaware Geological Survey, 5 pp.

Bockholt, B. M., C. A. Langston, and M. Withers (2015). Local magnitude and anomalous amplitude distance decay in the eastern Tennessee seismic zone, *Seismol. Res. Lett.* **86,** 1040–1050.

Chapman, M. C. (2013). On the rupture process of the 23 August 2011 Virginia earthquake, *Bull. Seismol. Soc. Am.* **103,** 613–628, doi: 10.1785/0120120229.

Dengler, L. A., and J. W. Dewey (1998). An intensity survey of households affected by the Northridge, California, earthquake of 17 January 1994, *Bull. Seismol. Soc. Am.* **88,** 441–462.

Du, W.-X., W.-Y. Kim, and L. R. Sykes (2003). Earthquake source parameters and state of stress for northeastern United States and southeastern Canada from analysis of regional seismograms, *Bull. Seismol. Soc. Am.* **93,** 1633–1648.

Electric Power Research Institute (EPRI) (2012). *Technical Report: Central and Eastern United States Seismic Source Characterization for Nuclear Facilities (lead Kevin J. Coppersmith)*, EPRI, U.S. DOE, and U.S. NRC, Palo Alto, California.

Frankel, A., A. McGarr, J. Bicknell, J. Mori, L. Seeber, and E. Cranswick (1990). Attenuation of high-frequency shear waves in the crust: Measurements from New York state, South Africa, and southern California, *J. Geophys. Res.* **95,** no. B11, 17,441–17,457.

Gibbons, S. J., and F. Ringdal (2006). The detection of low magnitude seismic events using array-based waveform correlation, *Geophys. J. Int.* **165,** no. 1, 149–166, doi: 10.1111/j.1365-246X.2006.02865.x.

Harris, D. B. (1991). A waveform correlation method for identifying quarry explosions, *Bull. Seismol. Soc. Am.* **81,** 2395–2418.

Herrmann, R. B. (1979). Surface wave focal mechanisms for eastern North American earthquakes with tectonic implications, *J. Geophys. Res.* **84,** 3543–3552.

Horton, J. W., Jr., A. A. Drake Jr., D. W. Rankini, and R. D. Dallmeyer (1991). Preliminary tectonostratigraphic terrane map of the central and southern Appalachians, *U.S. Geological Survey Miscellaneous Investigations Series Map I-2163*, scale 1:2,000,000.

Hough, S. E. (2012). Initial assessment of the intensity distribution of the 2011 M_w 5.8 Mineral, Virginia, earthquake, *Seismol. Res. Lett.* **83,** no. 4, 649–657.

Kim, W.-Y. (1998). The M_L scale in eastern North America, *Bull. Seismol. Soc. Am.* **88,** 935–951.
Kim, W.-Y. (2013). Induced seismicity associated with fluid injection into a deep well in Youngstown, Ohio, *J. Geophys. Res.* **118,** 3506–3518, doi: 10.1002/jgrb.50247.
Kim, W.-Y., and M. Chapman (2005). The 9 December 2003 central Virginia earthquake sequence: A compound earthquake in the central Virginia seismic zone, *Bull. Seismol. Soc. Am.* **95,** 2428–2445.
Kim, W.-Y., and K.-H. Kim (2014). The 9 February 2010, Siheung, Korea, earthquake sequence: Repeating earthquakes in a stable continental region, *Bull. Seismol. Soc. Am.* **104,** 551–559.
Klein, F. W. (2007). User's guide to HYPOINVERSE-2000, a Fortran program to solve for earthquake locations and magnitudes, *U.S. Geol. Surv. Open-File Rept. 02-171*, 121 pp.
McNamara, D. E., H. M. Benz, R. B. Herrmann, E. A. Bergman, and M. Chapman (2014). The M_w 5.8 central Virginia seismic zone earthquake sequence of August 23, 2011: Constraints on earthquake source parameters and fault geometry, *Bull. Seismol. Soc. Am.* **104,** 40–54, doi: 10.1785/0120130058.
Nuttli, O. W. (1973). Seismic wave attenuation and magnitude relations for eastern North America, *J. Geophys. Res.* **78,** 876–885, doi: 10.1029/JB078i005p00876.
Petersen, M. D., M. P. Moschetti, P. M. Powers, C. S. Mueller, K. M. Haller, A. D. Frankel, Y. Zeng, S. Rezaeian, S. C. Harmsen, O. S. Boyd, *et al.* (2014). Documentation for the 2014 update of the United States national seismic hazard maps, *U.S. Geol. Surv. Open-File Rept. 2014-1091*, 243 pp., doi: 10.3133/ofr20141091.
Pratt, T. L., J. W. Horton Jr., J. Muñoz, S. E. Hough, M. C. Chapman, and C. G. Olgun (2017). Amplification of earthquake ground motions in Washington, DC, and implications for hazard assessments in central and eastern North America, *Geophys. Res. Lett.* **44,** no. 24, 12,150–12,160, doi: 10.1002/2017GL075517.
Ramsey, K. W. (2007). Geologic map of Kent County, Delaware, *Delaware Geological Survey Map Series No. 14*, scale 1:100,000.
Roman, D. C., L. S. Wagner, T. Bartholomew, S. Golden, and B. Schleigh (2017). The Carnegie Quick Deploy Box (QDB) for use with broadband and intermediate period sensors, presented at the *2017 AGU Fall Meeting*, New Orleans, Louisiana, 11–15 December, Abstract S11C–0614.
Schaff, D. P. (2008). Semiempirical statistics of correlation-detector performance, *Bull. Seismol. Soc. Am.* **98,** 1495–1507.
Schaff, D. P., and P. G. Richards (2011). On finding and using repeating seismic events in and near China, *J. Geophys. Res.* **116,** no. B03309, doi: 10.1029/2010JB007895.
Seeber, L., J. G. Armbruster, W. Y. Kim, N. Barstow, and C. Scharnberger (1998). The 1994 Cacoosing Valley earthquakes near Reading, Pennsylvania: A shallow rupture triggered by quarry unloading, *J. Geophys. Res.* **103,** 24,505–24,521.
Slinkard, M., D. Schaff, N. Mikhailova, S. Heck, C. Young, and P. G. Richards (2014). Multistation validation of waveform correlation techniques as applied to broad regional monitoring, *Bull. Seismol. Soc. Am.* **104,** 2768–2781.
Soto-Cordero, L, A. Meltzer, and J. C. Stachnik (2018). Crustal structure, intraplate seismicity, and seismic hazard in the mid-Atlantic United States, *Seismol. Res. Lett.* **89,** 241–252.
Stover, C. W., and J. L. Coffman (1993). Seismicity of the United States, 1568–1989 (revised), *U.S. Geol. Surv. Profess. Pap. 1527*, 418 pp.
Sykes, L. R., J. G. Armbruster, W.-Y. Kim, and L. Seeber (2008). Observations and tectonic setting of historic and instrumentally-located earthquakes in greater New York City-Philadelphia area, *Bull. Seismol. Soc. Am.* **98,** 1696–1719.
Volkert, R. A., A. A. Drake Jr., and P. J. Sugarman (1996). Geology, geochemistry, and tectonostratigraphic relations of the crystalline basement beneath the coastal plain of New Jersey and contiguous areas, *U.S. Geol. Surv. Profess. Pap. 1565-B*, 48 pp.
Waldhauser, F. (2001). HypoDD—A program to compute double-difference hypocenter locations, *U.S. Geol. Surv. Open-File Rept. 2001-113*, 25 pp.
Waldhauser, F., and W. L. Ellsworth (2002). Fault structure and mechanics of the Hayward fault, California, from double-difference earthquake locations, *J. Geophys. Res.* **107,** 2054, doi: 10.1029/2000JB000084.
Wells, D., J. A. Egan, D. G. Murphy, and T. Paret (2015). Ground shaking and structural response of the Washington Monument during the 2011 Mineral, Virginia, earthquake, in *The 2011 Mineral, Virginia, Earthquake, and Its Significance for Seismic Hazards in Eastern North America*, J. W. Horton, M. C. Chapman Jr., and R. A. Green (Editors), *Geol. Soc. Am. Spec. Pap.* 509, 35 pp., doi: 10.1130/2015.2509(12).
Worden, C. B., M. C. Gerstenberger, D. A. Rhoades, and D. J. Wald (2012). Probabilistic relationships between ground-motion parameters and modified Mercalli intensity in California, *Bull. Seismol. Soc. Am.* **102,** 204–221.
Zhao, L. S., and D. V. Helmberger (1994). Source estimation from broadband regional seismograms, *Bull. Seismol. Soc. Am.* **84,** 91–104.

Won-Young Kim
Mitchell Gold
Joseph Ramsay
Lamont–Doherty Earth Observatory of Columbia University
Palisades, New York 10964 U.S.A.
wykim@LDEO.columbia.edu

Anne Meltzer
Earth and Environmental Sciences
Lehigh University
Bethlehem, Pennsylvania 18015 U.S.A.
ameltzer@lehigh.edu

David Wunsch
Stefanie Baxter
Delaware Geological Survey
257 Academy Street
University of Delaware
Newark, Delaware 19716 U.S.A.
dwunsch@udel.edu

Vedran Lekic
Phillip Goodling
Karen Pearson
Department of Geology
University of Maryland
College Park, Maryland 20742 U.S.A.
ved@umd.edu

Lara Wagner
Diana Roman
Department of Terrestrial Magnetism
Carnegie Institution for Science
Washington, D.C. 20015 U.S.A.
lwagner@carnegiescience.edu

Thomas L. Pratt
U.S. Geological Survey
12201 Sunrise Valley Drive
Reston, Virginia 20192 U.S.A.
tpratt@usgs.gov

Published Online 19 September 2018